CHALMERS
UNIVERSITY OF TECHNOLOGY

Effective Inertia Constant: A Frequency-Strength Indicator For Converter-Dominated Power Grids

Citation for the original published paper (version of record):
Imgart, P., Chen, P. (2023). Effective Inertia Constant: A Frequency-Strength Indicator For Converter-Dominated Power Grids. 2023 IEEE Belgrade PowerTech, PowerTech 2023. http://dx.doi.org/10.1109/POWERTECH55446.2023.10202722

Effective Inertia Constant: A Frequency-Strength Indicator For Converter-Dominated Power Grids

Paul Imgart
Division of Electric Power Engineering
Chalmers University of Technology
Göteborg, Sweden
paul.imgart@chalmers.se

Peiyuan Chen
Division of Electric Power Engineering
Chalmers University of Technology
Göteborg, Sweden
peiyuan@chalmers.se

***Abstract*—The system inertia constant is the predominant indicator for power system frequency strength, but fails to account for non-inertial contributions such as fast frequency response. In this paper, the effective inertia constant is proposed as a new indicator to account for the contribution from both synchronous generators and power-electronic interfaced sources. Time-domain simulations show that the effective inertia constant is a better indicator for frequency nadir than the conventional inertia constant.**

***Index Terms*—Frequency nadir, inertia, load-frequency control, power system stability, renewables integration**

I. Introduction

Frequency stability denotes the ability of a power system to maintain the frequency of its electric quantities within stipulated limits when subject to an active power imbalance [1]. Frequency deviations are typically arrested by frequency containment reserve (FCR) [2], [3]. The sensitivity of the system frequency prior to any control action like FCR activation depends on the amount of mechanical inertia coupled to the grid, with a higher amount of inertia resulting in a stiffer frequency [4]. Due to this, the system's inertia constant is today the main indicator of short term frequency strength, where short term refers to the time frame before a substantial amount of FCR has been activated, corresponding to the first $5\,\mathrm{s}$ to $15\,\mathrm{s}$ after a larger disturbance [3].

The efforts of decarbonizing the electricity sector have led to an increasing share of renewable energy sources in power systems throughout the world [5]. Among these, wind and solar power have shown the highest growth rates. They are predominantly interfaced to the grid through power electronic converters, in contrast to the conventional power plants they replace, which commonly contain synchronous machines (SMs) connected directly to the grid. Unlike the SMs, power converter-interfaced generation does not directly contribute to the system's inertia, which means a shift of generation from conventional to wind and solar results in a reduced system inertia [4], [6], [7]. Virtual inertia (VI) and fast frequency reserve (FFR) are two concepts used by converter-interfaced generation and storages to remedy this decrease in synchronously coupled mechanical inertia by providing controlled fast frequency support (FFS) [3], [7]–[12].

The utilization of FFS implicates that the short term frequency progression following a disturbance is no longer determined by the inertial response of the SMs and the load-frequency dependence alone. As a result, the value of the inertia constant as an indicator for frequency strength decreases. Since it is important for system operators to know the frequency strength of their system, a new indicator for frequency strength that incorporates the impact of FFS is needed.

Consequently, this paper proposes and evaluates an alternative indicator for the short term frequency strength of the bulk power system that reflects FFS from all sources non-discriminatorily. The proposed frequency strength indicator is referred to as the effective inertia constant. Section II summarizes different mechanism of frequency support from SMs and power-electronic interfaced sources (PEIS), and introduces measures quantifying the contribution of single units during a frequency disturbance. In Section III, measures and indicators for the frequency strength of the bulk power system are presented and the effective inertia constant is defined. It is followed by a case study of a generic power system with a varying degree of converter-interfaced generation in Section IV and V, demonstrating the capability of the newly suggested frequency strength indicator to include FFS from PEIS.

II. Inertial and Fast Frequency Support

Inertial support describes the natural reaction of SMs to a frequency change as well as the control action of those PEIS with VI, while FFS refers to frequency control faster than FCR, typically provided by converter-interfaced resources. In this section, both mechanisms of frequency support as well as two measures to quantify an individual unit's contribution to it are presented.

A. Inertial Frequency Support

The inertial support provided by a SM is governed by the swing equation, which in pu is expressed as

$$2H\frac{\mathrm{d}\omega}{\mathrm{d}t} = T_\mathrm{m} - T_\mathrm{e} = \frac{P_\mathrm{m} - P_\mathrm{e}}{\omega}, \tag{1}$$

where H is the inertia constant in s, ω the rotor speed, T_m the mechanical and T_e the electrical torque, P_m the mechanical and P_e the electrical power [13].

B. Fast Frequency Support (FFS)

In contrast to inertial support from SMs, FFS from PEIS is not dictated by physical behaviour like the swing equation does for SMs, but instead is a design choice within the limits of the source's power and energy reserves. The different strategies for inertial support are commonly categorized into three groups [14], [15], depending on the quantity used to control the FFS power, which can be

1) independent of the frequency but follow a predefined support profile once a frequency deviation threshold is passed and the support is activated,
2) proportional to the frequency deviation, resembling a FCR droop controller, or
3) based on the rate of change of frequency (RoCoF), emulating the inertial response of a SM.

Depending on the selected approach, the support from the unit to the grid has to be estimated differently. In this work, an approach based on ENTSO-E's Nordic region FFR specification is investigated [3], with the corresponding support profile described in detail in Section IV. The chosen approach is frequency-independent.

C. Frequency Strength Measures on Unit Level

The impact of a single unit on the system frequency strength can be quantified by two unit-level frequency strength measures, which are estimated examining the unit's response to a stiff frequency. The first measure is the specific FFS power $\overline{P}_{\mathrm{FFS}}$ and is defined as

$$\overline{P}_{\mathrm{FFS}} = \frac{P - P_0}{P_0}, \tag{2}$$

where P denotes the quasi-steady state active power injection from the unit into the grid and P_0 the pre-disturbance power injection. This means a unit with a $\overline{P}_{\mathrm{FFS}} = 0.2$ injects an additional $20\,\%$ of its pre-disturbance power during a frequency disturbance.

The second measure is the specific FFS energy $\overline{E}_{\mathrm{FFS}}$, which is at time t defined as

$$\overline{E}_{\mathrm{FFS}}(t) = \int_{t_0}^{t} \frac{P - P_0}{P_0} = \frac{E(t) - E_0(t)}{E_0(t)}, \tag{3}$$

with t_0 the time the disturbance occurs, $E(t)$ the energy that is injected into the grid from begin of the disturbance until t and $E_0(t)$ the energy that would have been injected over the same time by keeping the active power constant as P_0. In the rest of this study the term specific FFS energy will refer to the maximum of $\overline{E}_{\mathrm{FFS}}$ for a given disturbance, thus eliminating the variation over time.

For a SM, these measures can be calculated using (1), assuming that the mechanical power is constant:

$$\overline{P}_{\mathrm{FFS}} = -\frac{2H}{P_0}\omega\frac{\mathrm{d}\omega}{\mathrm{d}t} \quad \text{and} \tag{4}$$

$$\overline{E}_{\mathrm{FFS}} = \frac{H}{P_0}(\omega_0^2 - \omega_{\min}^2), \tag{5}$$

where P_0 is the pre-disturbance active power output, ω_0 is the pre-disturbance and $\omega_{\min}$ the minimum rotor speed in pu, respectively. For the contribution from units participating in FFR, the estimation of these values depends on the chosen FFR approach.

III. System Level Frequency Strength Measures and Indicators

In this section, measures and indicators for the frequency strength of the bulk power system are presented. Those quantities denoted as measures are generally related to specific disturbances and can directly be measured, while those referred to as indicators can not be measured directly, but give a more general, less disturbance-specific assessment of the system frequency strength. Assuming that no generator loses synchronism, no system separation occurs and the frequency can be considered a global system quantity, the individual SMs in the system can be aggregated through their swing equations (1) to yield the lumped mass model given by

$$2H_{\mathrm{sys}} f \frac{\mathrm{d}f}{\mathrm{d}t} = P_{\mathrm{m}} - P_{\mathrm{e}}, \tag{6}$$

where

$$H_{\mathrm{sys}} = \frac{\sum H S_{\mathrm{r}}}{S_{\mathrm{b,sys}}} \tag{7}$$

is the equivalent system inertia constant in s under the total system base apparent power $S_{\mathrm{b,sys}}$. f denotes the system frequency, P_{m} the total mechanical power input and P_{e} the total active electrical power consumption, including both the frequency-independent and frequency-dependent load, all in pu. As suggested in [16], the reduction in inertia due to converter-interfaced generation can be considered by including their rated power in $S_{\mathrm{b,sys}}$, but with zero inertia constant.

A. Direct Measures of System Frequency Strength

The frequency strength of a power system is directly reflected by the frequency excursion caused by a given disturbance in the power balance. There exist a variety of measures to quantify this [6], [17], but the most commonly used ones include rate of change of frequency (RoCoF), frequency nadir and time to nadir. These three measures are illustrated in Fig. 1. There exist further metrics such as steady-state frequency deviation and damping of the frequency after

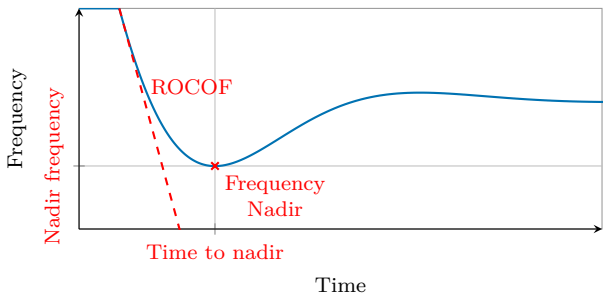

Fig. 1: Direct measures of system frequency strength.

the response [17]. These are not relevant for the phenomena described in this work and therefore not described in detail.

B. Frequency Strength Indicators

In contrast to the disturbance-specific measures presented in the previous section, a frequency strength indicator is representing the overall system strength independently of a specific disturbance, i.e. the stiffness of the system frequency in the face of power imbalances, the size of resulting frequency deviations and the stability margins of the system. The classical indicator for frequency strength in use today is the system inertia constant H_{sys} [6], [17]. It affects both the RoCoF as shown in (6) as well as the frequency nadir of the power system due to the time delay of FCR action, and thereby serves as a good indication of the frequency strength. However, as H_{sys} represents exclusively inertial support it fails to accurately indicate the frequency strength of systems incorporating other means of FFS.

A possible solution is to include these alternate sources of FFS based on the energy they deliver. This energy can be compared to the energy that a SM would deliver for a given minimum frequency. This results in the proposal of the effective inertia constant: The inertia constant of a SM supporting with the same amount of energy when subjected to the same frequency deviation. It can be estimated as

$$H_{\mathrm{eff}} = \frac{\overline{E}_{\mathrm{FFS}} P_0}{f_0^2 - f_{\mathrm{min}}^2} \tag{8}$$

with the pre-disturbance frequency f_0 and minimum frequency f_{min}. This allows to include sources of FFS when estimating the system inertia constant with the help of (7). This proposed new indicator comes with some caveats:

- The FFS included via H_{eff} has to act on a similar time scale as the SM's inertial response and should be distinct from other means of frequency control. The analogy to an inertial response is most accurate if the deadband for the activation of FFS is as small as possible and the support energy considered in the calculation is delivered before the frequency nadir is reached.
- As defined in (8), the effective inertia constant depends on f_{min}. In case of FFS sources that support with a fixed amount of energy independent of the frequency deviation, the support given to the grid will be larger than expected if the deviation in frequency is smaller than what was used to calculate the effective inertia constant. If the deviation is larger, the support will be smaller than what is expected. Thus, this parameter should be chosen carefully.

IV. Description of Simulation Model

A case study of a single disturbance with varying degrees of wind power production and FFR provision is conducted in MATLAB to assess and compare the suitability of the proposed effective inertia constant and the classical system inertia constant to capture the system frequency strength.

A. Lumped Mass Model and Modelling of FCR

Assume that the power system is modelled as a one-mass model. The linearized swing equation in Laplace domain can be expressed as [13]

$$2H_{\mathrm{sys}} s \Delta f = \Delta P_{\mathrm{m}} - \Delta P_{\mathrm{e}} \tag{9}$$

where Δf is the variation in system frequency, ΔP_{m} the variation in mechanical power and ΔP_{e} the variation in electrical power. The mechanical power is the total mechanical power of the SMs in the system, while the electrical power represents the residual load, i.e. the load minus the generation from converter-interfaced renewable generation, import through HVDC links and power injection from energy storage. The system inertia constant H_{sys} is estimated with the synchronous generation active power P_{syn}, power factor $\cos\varphi$ and inertia constant H_{syn} according to (7) and [14] as

$$H_{\mathrm{sys}} = \frac{H_{\mathrm{syn}} P_{\mathrm{syn}}}{S_{\mathrm{b,sys}} \cos\varphi}, \tag{10}$$

where converter-interfaced generation is considered in $S_{\mathrm{b,sys}}$.

The present model can be extended to include the load frequency dependency [13], which is determined by the load damping constant D and can be taken into account through

$$(2H_{\mathrm{sys}} s + D)\Delta f = \Delta P_{\mathrm{m}} - \Delta P_{\mathrm{l}}, \tag{11}$$

where ΔP_{l} denotes the frequency-independent change in residual load. Furthermore, the model should include the FCR, which is a control action of the SM governors due to a frequency deviation. Simplifying the approach presented in [17], it can be modelled as a first-order system following

$$\Delta P_{\mathrm{FCR}} = -\frac{1}{R} \frac{1}{T_{\mathrm{FCR}} s + 1} \Delta f, \tag{12}$$

where ΔP_{FCR} is the variation in the FCR activation in pu, R is the droop constant and T_{FCR} is the FCR activation time constant. To represent that not all SMs in the system participate in the FCR, the droop constant R should be replaced by the effective droop

$$R_{\mathrm{eff}} = R \frac{S_{\mathrm{b,sys}}}{P_{\mathrm{FCR,tot}}}, \tag{13}$$

where $P_{\mathrm{FCR,tot}}$ is the total available frequency containment reserve (FCR). The activated FCR is limited to $P_{\mathrm{FCR,tot}}$ and then applied as a mechanical power deviation in (11). The parameters of the system model are shown in Table I and are selected to reproduce a system behaviour similar to the tuning disturbance in [17]. In accordance with the reference, only the component of FCR designed for large disturbances is taken into consideration in this model, FCR-D.

B. Modelling of FFR

In this paper, FFR from PEIS is implemented similar to the ENTSO-E specification [18]. As a result, the FFR is considered directly a change in the electrical power, as it is independent of the frequency once activated. It is activated at a frequency of $49.7\,\mathrm{Hz}$ and ramped up to $100\,\%$ in $1.3\,\mathrm{s}$.

TABLE I: Simulation model parameters.

Parameter	Value
SM inertia constant H_{syn}	4.5 s
Synchronous generation power factor	0.8
PEIS inertia constant H_{wind}	0 s
PEIS power factor	1
Load damping constant D	1 %
Droop constant R	0.8 %
FCR time constant T_{FCR}	20 s
FCR activation threshold	49.9 Hz
FFR activation threshold	49.7 Hz

Short-duration FFR is chosen here, which according to [18] has to be supplied for a duration of 2 s. The contribution is then reduced to 0 % over the time of 10 s. The recovery begins after a buffer time of 15 s from the deactivation of the FFR support and is limited to 25 % of the FFR contribution in power. Due to potential losses, more energy needs to be recovered than injected during FFR [19]. To account for this, the length of the recovery period is calculated to result in a 20 % higher energy transfer than during the support period. This results in a recovery time of approximately 40 s. The FFR activation and recovery is illustrated in Fig. 2.

The selected, frequency-independent approach means that $\overline{P}_{\text{FFS}}$ is determined solely by the requirements and controller design, and is selected to be 3 % of the wind turbines' active power, which is well within the capabilities reported in [19]. The specific FFS energy can be estimated as

$$\overline{E}_{\text{FFS}} = \overline{P}_{\text{FFS}}(t_{\text{sup}} + \frac{t_{\text{ramp}}}{2}), \tag{14}$$

where t_{sup} denotes the time the full FFR power is provided, and t_{ramp} the total ramp time during activation and deactivation. Apart from the described FFR, the wind turbines in this model do not provide other forms of FFS, VI or FCR. The resulting model for the case study simulation is shown in Fig. 3.

V. Simulation Results

A. Description of Case Studies

Table II lists five simulated cases with varying wind power penetration and FFR provision. The system load is 50 GW in all cases. The first case is a base case, where the load is entirely supplied from synchronous generators. For the other cases, part of the synchronous generation is replaced by wind power, which results in a reduced kinetic energy and system

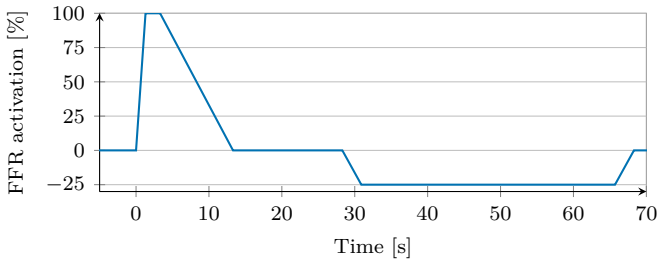

Fig. 2: Modelled FFR activation and recovery.

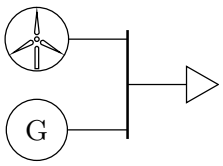

a) Illustration of the lumped mass simulation model.

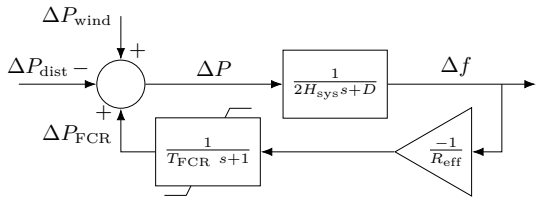

b) Block diagram of the lumped mass simulation model.

Fig. 3: Lumped mass system model for the case study.

inertia constant. In case 2 and 4, no FFR is delivered, and in case 3 and 5, the wind turbines support with 3 % of their active power as FFR. The disturbance applied is the same for all cases. It is dimensioned to lead to a frequency nadir of approximately 49.5 Hz in the base case and is close to the dimensioning fault for the Nordic system.

TABLE II: Simulation cases.

Parameter	Case 1	Case 2	Case 3	Case 4	Case 5
Synchr. generation (GW)	50	40	40	30	30
Wind power (GW)	0	10	10	20	20
Kinetic energy (GW s)	281.25	225	225	168.75	168.75
FCR-D (MW)	1450	1450	1450	1450	1450
FFR (MW)	0	0	300	0	600
Disturbance (MW)	1070	1070	1070	1070	1070

B. Proposed System Effective Inertia Constant

Fig. 4 shows the simulated frequency, FCR and FFR activation. The frequency measures and indicators introduced in Section III are estimated for each of the cases and summarized in Table III. The RoCoF is estimated over an average of 5 electrical cycles [14]. Fig. 4 shows that the RoCoF is the highest at the beginning of the disturbance, before any reserves are activated. Thus, the maximum RoCoF is only affected by the kinetic energy in the system, with higher RoCoF in case of a lower system kinetic energy [12].

TABLE III: System frequency strength measures and indicators for the simulated case study.

Measure	Case 1	Case 2	Case 3	Case 4	Case 5
Max. RoCoF (Hz/s)	0.0935	0.1165	0.1165	0.1545	0.1545
Frequency nadir (Hz)	49.5	49.47	49.57	49.42	49.56
Time to nadir (s)	11.89	10.27	12.07	8.5	18.44
H_{sys} (s)	4.5	3.75	3.75	2.93	2.93
$H_{\text{wind,eff}}$ (s)	0	0	5.8	0	5.8
$H_{\text{sys,eff}}$ (s)	4.5	3.75	4.72	2.93	4.95

For the cases not involving any FFR (cases 1, 2 and 4), the consequence of a reduced kinetic energy (as represented by H_{sys}) is a lower frequency nadir and shorter time to nadir. In these cases the inertia constant H_{sys} gives a good indication of the frequency strength of the system. In case 3 and 5, which include FFR support from the wind turbines, this is

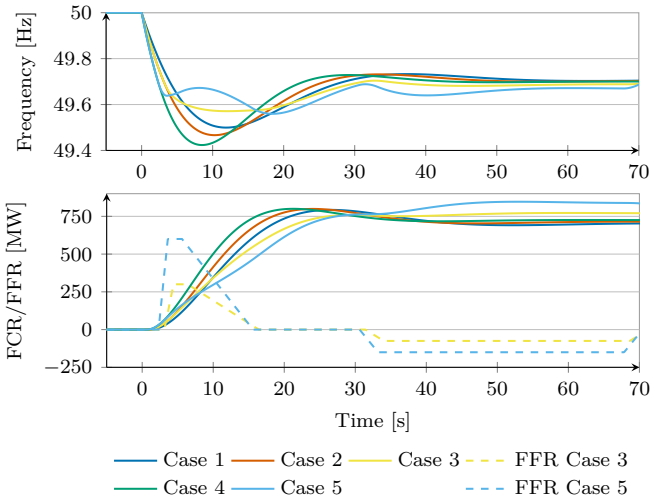

Fig. 4: Simulated frequency, FCR and FFR activation.

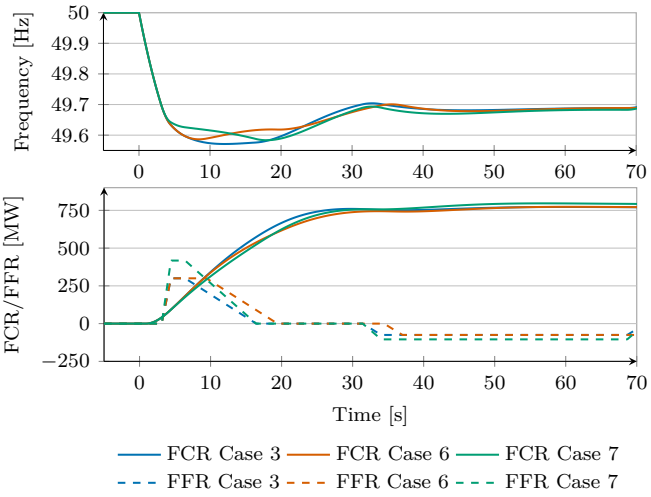

Fig. 5: Simulation results for the case study with varied FFR.

no longer true. Even though the system inertia constant is decreasing, both nadir and time to nadir are not following this trend. As seen in Fig. 4, in case 5 the nadir occurs when the FFR is ramped down. However, even this secondary dip occurs at a notably higher frequency than in the no-FFR cases. Hence H_{sys} does not give a reliable estimation of the system frequency strength in these cases since the contribution from FFR is disregarded in the indicator, which confirms the concern presented in Section III.

The effective inertia constant $H_{\text{wind,eff}}$ is here estimated with a minimum frequency of $49\,\text{Hz}$, which is the minimum allowable instantaneous frequency in the Nordic power system. The resulting effective system inertia constant is estimated using (7) and $H_{\text{wind,eff}}$ as the wind turbine inertia constant. Since $H_{\text{wind,eff}}$ for the chosen FFR strategy is larger than the SMs' inertia constant, an increasing share of wind power results in an increasing effective system inertia constant. This corresponds well with an increasing time to nadir. The nadir does not follow the same trend, as it is lower in case 5 than in case 3. This is due to the secondary dip during the FFR deactivation though, which means that the indicator is reliable for the first dip. Fine-tuning and coordinating the different frequency controls present in a system is a must, especially if a new type of control such as FFR is introduced. As the coordinated frequency control is not the main purpose of this study the demonstrated behaviour is acceptable here.

C. Impact of the Shape of FFR Provision

To be able to judge how the shape of the FFR support affects the informative value of the proposed frequency strength indicator H_{eff}, two additional cases with altered FFR specifications are simulated, with parameters listed in Table IV. Case 3 from the previous study is included as a base case for comparison. For case 6, the duration of full power FFR support was increased from $2\,\text{s}$ to $5\,\text{s}$, which corresponds to the time given in [18]. For case 7, the time was kept at $2\,\text{s}$, but in return the FFR contribution was increased so that approximately the same amount of FFS energy is supplied, resulting in nearly the same effective inertia constants as in case 6. This increase results in a specific FFS power $\overline{P}_{\text{FFS}}$ of $4.175\,\%$ in contrast to $3\,\%$ in the other cases.

TABLE IV: Simulation cases with varying FFR specification.

Parameter	Case 3	Case 6	Case 7
FFR (MW)	300	300	417.5
FFR support time (s)	2	5	2

The results of this case study are shown in Fig. 5 and in Table V. The frequency nadir is higher in both case 6 and 7 than in the base case, and differs only very slightly between those two cases. In contrast, the time to nadir varies greatly even between the cases with increased FFS: In case 6 the primary dip is dominant, due to the prolonged FFR provision bridging the time until more FCR has activated. This means the decrease in frequency can be stopped earlier than in case 3, where FFR starts to ramp down before the nadir is reached. The secondary dip occurs only slightly in case 6 and at an already higher frequency, resulting in the lowest time to nadir. In case 7 on the other hand, the higher FFR support results in an earlier slow down of the frequency change. Due to the short time of the support it ends before FCR has activated sufficiently to take over, which becomes visible in the pronounced secondary frequency dip.

TABLE V: Results for cases with varying FFR specification.

Measure	Case 3	Case 6	Case 7
Max. RoCoF	$0.1165\,\text{Hz/s}$	$0.1165\,\text{Hz/s}$	$0.1165\,\text{Hz/s}$
Frequency nadir	$49.57\,\text{Hz}$	$49.59\,\text{Hz}$	$49.58\,\text{Hz}$
Time to nadir	$12.07\,\text{s}$	$8.45\,\text{s}$	$17.99\,\text{s}$
H_{sys}	$3.75\,\text{s}$	$3.75\,\text{s}$	$3.75\,\text{s}$
$H_{\text{wind,eff}}$	$5.8\,\text{s}$	$8.07\,\text{s}$	$8.07\,\text{s}$
$H_{\text{sys,eff}}$	$4.72\,\text{s}$	$5.09\,\text{s}$	$5.09\,\text{s}$

D. Suitability of the Effective Inertia Constant

As the effective inertia constant includes the impact of non-inertial FFS, it does not correlate well with the maxi-

mum RoCoF. However, there is a good correlation with the frequency nadir and in some cases even with the time to nadir. The Pearson correlation coefficient between $H_{\mathrm{sys,eff}}$ and the frequency nadir is 0.96 over all simulation cases, which indicates a very strong linear correlation even though the FFR specification was varied for case 6 and 7. The same coefficient drops to 0.19 if the classical indicator H_{sys} is used instead. These findings have also been confirmed for different disturbance sizes. For the correlation between $H_{\mathrm{sys,eff}}$ and time to nadir, results vary depending on FFR specifications and disturbance sizes due to the interaction between FFR deactivation and FCR. To summarize, it can be observed that the effective inertia constant is a meaningful indicator for the frequency nadir of the presented study cases even when the specification of FFR is varied, as long as the FFR is mainly provided prior to the full FCR activation. Further studies are needed to investigate conditions for good correlation with the time to nadir, as well as comparability and sensitivity of the indicator for different FFR specifications and disturbance sizes.

VI. Conclusions and Further Work

This paper demonstrates the inadequacy of the system inertia constant as the sole indicator for system frequency strength in power systems containing FFS apart from inertial support. It proposes the effective inertia constant as a new indicator for power system frequency strength to reflect these other contributions. The ability of the effective inertia constant to capture the system frequency strength even in the presence of FFR is demonstrated. Care has to be taken if the system is prone to secondary frequency dips during deactivation or recovery of the FFR, as these can result in lower frequencies than the original disturbance and are not covered by the effective inertia constant. The presented simulations demonstrate that the effective inertia constant is, within limits, even able to indicate the frequency nadirs if different specifications for FFR are used. As an additional result, FFS from wind turbines with existing FFR specifications is shown to correspond to an effective inertia constant of $5.8\,\mathrm{s}$, similar to those of large conventional power stations. This is the case even though a very low FFR contribution of only $3\,\%$ of the turbine's pre-disturbance active power was considered and a very low minimum frequency of $49\,\mathrm{Hz}$ was used to estimate the effective inertia constant. Future work is required to further explore the applicability of the suggested frequency indicator across different systems at different system operating points, in particular for varying composition of generation. The need of other control strategies for FFR should be investigated in the future for wind power penetration exceeding $50\,\%$.

References

[1] P. Kundur *et al.*, "Definition and Classification of Power System Stability IEEE/CIGRE Joint Task Force on Stability Terms and Definitions," *IEEE Transactions on Power Systems*, vol. 19, no. 3, Aug. 2004.

[2] ENTSO-E, "Appendix 1: Load-Frequency Control and Performance," in *UCTE Operation Handbook*, 2004.

[3] ENTSO-E Nordic Region, *Nordic System Operation Agreement – Annex Load-Frequency Control & Reserves*, 2020.

[4] P. Tielens *et al.*, "The relevance of inertia in power systems," *Renewable and Sustainable Energy Reviews*, vol. 55, Mar. 2016.

[5] International Energy Agency, "Electricity Information," 2020.

[6] C. Seneviratne *et al.*, "Frequency response due to a large generator loss with the increasing penetration of wind/PV generation – A literature review," *Renewable and Sustainable Energy Reviews*, vol. 57, May 2016.

[7] J. Matevosyan *et al.*, "Grid-Forming Inverters: Are They the Key for High Renewable Penetration?" *IEEE Power and Energy Magazine*, vol. 17, no. 6, Nov. 2019.

[8] I. Erlich *et al.*, "Impact of large wind power generation on frequency stability," in *Power Engineering Society General Meeting, 2006. IEEE*, IEEE, 2006.

[9] L. Ruttledge *et al.*, "Frequency Response of Power Systems With Variable Speed Wind Turbines," *IEEE Transactions on Sustainable Energy*, vol. 3, no. 4, 2012.

[10] L. Wu *et al.*, "Towards an Assessment of Power System Frequency Support From Wind Plant - Modeling Aggregate Inertial Response," *IEEE Transactions on Power Systems*, vol. 28, no. 3, Aug. 2013.

[11] P. J. Vogler-Finck *et al.*, "Evolution of primary frequency control requirements in Great Britain with increasing wind generation," *International Journal of Electrical Power & Energy Systems*, vol. 73, Dec. 2015.

[12] R. Eriksson *et al.*, "Synthetic inertia versus fast frequency response: A definition," *IET Renewable Power Generation*, vol. 12, no. 5, 2018.

[13] P. Kundur, *Power System Stability and Control* (The EPRI Power System Engineering Series), N. J. Balu *et al.*, Eds. New York: McGraw-Hill, 1994.

[14] M. Persson, "Frequency Response by Wind Farms in Power Systems with High Wind Power Penetration," Chalmers University of Technology, Göteborg, 2017.

[15] IEEE, *P2800/D6.0 (March 2021) - Draft Standard for Interconnection and Interoperability of Inverter-Based Resources Interconnecting with Associated Transmission Systems*, Mar. 2021.

[16] M. Persson *et al.*, "Frequency control by variable speed wind turbines in islanded power systems with various generation mix," *IET Renewable Power Generation*, vol. 11, no. 8, 2017.

[17] ENTSO-E *et al.*, "Future system inertia 2," 2018.

[18] ENTSO-E *et al.*, "FFR Design of Requirements – External document," 2020.

[19] P. Imgart *et al.*, "Evaluation of the System-Aggregated Potentials of Inertial Support Capabilities from Wind Turbines," presented at the ISGT Europe 2019, Bucharest, 2019.